

Synthesis, Organo-Functionalization, and Catalytic Properties of Tungsten Oxide Nanoparticles As Heterogeneous Catalyst for Oxidative Cleavage of Oleic Acid As a Model Fatty Acid into Diacids

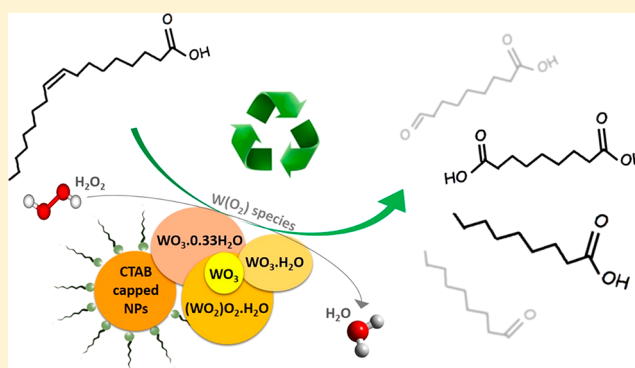
Amir Enferadi-Kerenkan,[†] Aimé Serge Ello,^{†,‡} and Trong-On Do^{*,†}

[†]Department of Chemical Engineering, Université Laval, Québec, G1V 0A6, Canada

[‡]Laboratoire de Chimie Physique, Université Félix Houphouët-Boigny de Cocody, 22 bp 582 Abidjan, Cote d'Ivoire

S Supporting Information

ABSTRACT: A series of tungsten oxide nanoparticles (NPs) has been synthesized via a green and straightforward approach exploiting bare tungsten powder as a precursor. The synthesized NPs were further organo-functionalized by cetyltrimethylammonium bromide (CTAB) in order to adjust their surface state and enhance their compatibility with biphasic oxidation of vegetable oils with H₂O₂. Simply, different structures of tungsten oxide were observed, which were characterized by XRD, FTIR, TGA, TEM, N₂ adsorption/desorption isotherms, and zeta potential analysis. All the synthesized nanocatalysts could fully convert oleic acid, and the highest yield of production of the desired diacid (azelaic acid), ~80%, was achieved by optimization of the CTA⁺ amount on the nanocatalyst's surface, which show excellent activity compared to the reported heterogeneous works. Thanks to the organo-functionalization, this water-tolerant catalyst exhibited no significant leaching, as well as convenient recovery and steady reuse without a noticeable decrease in activity, at least up to four cycles.



Thanks to the organo-functionalization, this water-tolerant catalyst exhibited no significant leaching, as well as convenient recovery and steady reuse without a noticeable decrease in activity, at least up to four cycles.

1. INTRODUCTION

Exploiting the synthetic capabilities of nature in oils and fats of vegetable and animal origin has rendered these renewable raw materials one of the key aspects of sustainable chemistry. Oleic acid (C18:1), the most widely distributed and abundant unsaturated fatty acid (UFA) in natural oils and fats,¹ can be oxidatively cleaved to produce azelaic (C9 diacid) and pelargonic (C9 monoacid) acids, which are rare in natural resources but very attractive materials, in particular the first one, for preparation of numerous products such as polymers (nylon-6:9), adhesives, biodegradable lubricants, corrosion inhibitors, antiacneic agents for cosmetics, perfumes, and resins.² Currently, this reaction is carried out in industry via ozonolysis, which, nowadays, has been converted to a controversial challenge due to the hazardous problems associated with use of ozone. Employing an eco-friendlier oxidant requires an active catalyst to be employed, as well.

Efforts in this context have focused on transition metals like Mo,³ Au,⁴ Mn, Cr,⁵ Co,^{5,6} Fe,^{7,8} Ru,^{9–13} and W,^{3,14–21} as catalytic cores, in homogeneous and heterogeneous forms, which have been thoroughly reviewed in our recent review paper.²² While the use of homogeneous catalysts has been well reported, curiously, heterogeneous ones have been scarcely investigated, probably due to the, often, much lower yields obtained by the latter. Hydrogen peroxide has always been an

interesting benign oxidant for the oxidation of olefins, especially when its use is associated with employing phase transfer agents via functionalization of the catalyst surface to improve compatibility of the aqueous oxidant and organic substrate. Although this could generally increase the efficiency of oxidation of UFAs,^{3,14–16,18,21} the major drawback is that the used catalytic system is not fully recoverable.

Among all the transition metals, tungsten has attracted a great deal of interest in the oxidation of UFAs, mostly in the W-based complex form and homogeneous catalysis. Solid W-based catalysts, however, include a variety of chemical structures arising from the distinct inherent properties of tungsten; varying oxidation states from -2 to $+6$ ²³ has led to several WO_x (x mainly between 2 and 3). The most common is tungsten trioxide, which in turn, includes hydrated (WO₃·nH₂O) and anhydrous (WO₃) forms. Moreover, peroxotungstic acid is another interesting structure that has shown great catalytic potential, particularly in oxidation reactions.²⁴ Formation of these different phases is very sensitive to synthesis conditions,²⁵ so the choice of a unique synthesis method that can produce all

Received: July 20, 2017

Revised: September 2, 2017

Accepted: September 7, 2017

Published: September 7, 2017

the phases is of importance. Oxidative dissolution of tungsten metal or tungstic acid in H_2O_2 was proposed by Kudo et al. to synthesize peroxotungstic acid²⁶ and then was modified to synthesize some other tungsten oxide structures.^{25,27–29} Recently, Ozin et al. developed this method to produce nanoparticles and thin films of tungsten oxide, as well as some other metal oxides.³⁰

In this work, different structures of tungsten oxide like $[(\text{WO}_2)_2\text{O}_2\cdot\text{H}_2\text{O}]$, WO_3 , $\text{WO}_3\cdot 0.33\text{H}_2\text{O}$, and $\text{WO}_3\cdot\text{H}_2\text{O}$ were synthesized via oxidative dissolution of micrometer-scale bare W powder, and then, these materials were examined in oxidative cleavage of oleic acid. In order to tune hydrophobicity/hydrophilicity properties of the surface and improve compatibility of the solid catalysts with the organic substrate and aqueous oxidant, the nanocatalysts were organo-functionalized by different amounts of cetyltrimethylammonium bromide (CTAB), a well-known cationic surfactant. Employing a simple and green synthesis method, that exploits cheap W powder as a precursor, avoided using time- and energy-consuming operations such as thermal treatment in an autoclave and purification, organic solvents, metal salts, and/or coordination compounds, which are commonly required in prior reported synthesis methods.

2. EXPERIMENTAL SECTION

2.1. Synthetic Details and Characterization. Tungsten oxide NPs were prepared by simple dispersion of metallic tungsten powder (1.0 g; APS 1–5 μm , purity 99.9%, Alfa Aesar Co.) in deionized H_2O (10 mL), followed by the addition of H_2O_2 (10 mL; aqueous solution, 30%, Fisher Scientific Co.) dropwise. The latter was done at 0 °C by keeping the reaction vessel in an instant ice bath. The oxidative dissolution process is very exothermic; therefore, it must be done with attention under a well-ventilated fume hood. After 4 h, an almost colorless (very slightly light yellow) and clear solution was formed (solution A). This solution was then allowed to precipitate through two different ways: (i) it was slowly evaporated at room temperature (RT) for 3 days (sample I), followed by calcination at 600 °C for 3 h (heating rate: 4 °C/min) under air to obtain sample II, or (ii) it was heated to 120 °C for 4 h in the absence of CTAB (sample III) and in the presence of CTAB (technical grade, Fisher Scientific Co.) with molar CTAB/W ratios of 0.1, 0.25, and 0.5 added to the solution just before heating (samples IV, V, and VI, respectively). Solid products were separated using a centrifuge at 8000 rpm, washed thoroughly with water and ethanol, and dried at 60 °C overnight (16 h). The used 1 g W gave ~1.1–1.6 g of products. The synthesized samples were characterized by XRD, FTIR, TGA and DTA, TEM, zeta potential analyzer, and BET surface area measurement. Section S1 in the Supporting Information explains the characterization equipment and methodologies.

2.2. Catalytic Test. The reactions were carried out in a 50 mL, round-bottom flask under a batch-wise constant temperature and constant pressure mode. This reactor was equipped with a condenser, a magnetic stirrer, and an oil bath. Typically, the reaction feed included 1 g of oleic acid ($\geq 99\%$, Sigma-Aldrich Co.), 4 mL of H_2O_2 , and 7.5 mL of *tert*-butanol ($\geq 99.0\%$, Sigma-Aldrich Co.) as a solvent. After adding 0.45 g of catalyst, the flask was put in the oil bath, which was previously heated and maintained at a constant temperature of 120 °C. During reaction, the reactor was continuously agitated with a magnetic stirrer (agitation rate ~400 rpm). After 5 h of

reaction, the catalyst was separated using a centrifuge at 8000 rpm and recovered via washing with ethanol and water several times and drying at 60 °C overnight to be used in the next catalytic cycle. The products mixture, then, underwent a derivatization reaction, in which the expectedly produced azelaic and pelargonic acids, and possibly unreacted oleic acid, were converted to their corresponding methyl esters according to the Metcalfe et al. derivatization procedure,^{31,32} in order to be prepared for GC-MS analysis.

Analysis of the reaction products by GC-MS has been explained in section S2 of the Supporting Information, covering detailed information about sample preparation prior to injection (section S2.1), quantitative analysis (section S2.2), and GC-MS specifications (section S2.3).

3. RESULTS AND DISCUSSIONS

3.1. Catalysts Synthesis and Characterization. Simply taking W powder, adding H_2O_2 , and then just altering the temperature of the thermal treatment and/or adding a surfactant, different catalytically interesting structures of tungsten oxide were achieved. Table 1 summarizes the synthesis conditions and prepared samples and shows their obtained crystalline phases and chemical structures.

Table 1. Synthesis Conditions and Prepared Samples

sample	CTAB/W molar ratio	synthesis ^a		crystalline phase	chemical structure
		T (°C)	t (h)		
I		RT ^b	72	monoclinic	$(\text{WO}_2)_2\text{O}_2\cdot\text{H}_2\text{O}$
II ^c		600	3	monoclinic	WO_3
III		120	4	orthorhombic	$\text{WO}_3\cdot 0.33\text{H}_2\text{O}$ and $\text{WO}_3\cdot\text{H}_2\text{O}$
IV	0.1	120	4	orthorhombic	$\text{WO}_3\cdot 0.33\text{H}_2\text{O} \gg \text{WO}_3\cdot\text{H}_2\text{O}$
V	0.25	120	4	orthorhombic	$\text{WO}_3\cdot 0.33\text{H}_2\text{O} \gg \text{WO}_3\cdot\text{H}_2\text{O}$
VI	0.5	120	4	orthorhombic	$\text{WO}_3\cdot 0.33\text{H}_2\text{O}$

^aSynthesis conditions: initial amounts of W elemental powder (1 g), H_2O (10 mL), H_2O_2 (10 mL), CTAB (0.20, 0.50, and 0.99 g for samples IV, V, and VI, respectively). ^bRT: room temperature ^cSample II: Sample I followed by calcination at 600 °C for 3 h.

3.1.1. Crystalline Structural Features. Fundamentally, oxidative dissolution of W powder in H_2O_2 gives an almost colorless and strongly acidic solution containing amorphous peroxotungstic acid particles, for which the empirical formula of $\text{WO}_3\cdot x\text{H}_2\text{O}_2\cdot y\text{H}_2\text{O}$ ($0.05 \leq x \leq 1$ and $3 \leq y \leq 4$) has been suggested in the literature.^{29,33} This solution, denoted as A, then underwent different crystallization approaches to achieve the catalytically desired structures of tungsten oxide. XRD patterns of the synthesized samples are shown in Figure 1. While rapid evaporation of solution A, expectedly, gave amorphous tungsten oxide, an interesting structure of peroxotungstic acid or hydrated tungsten peroxide $[(\text{WO}_2)_2\text{O}_2\cdot\text{H}_2\text{O}]$, which contains active oxidizing agent of tungsten-peroxo, was obtained by slow evaporation of the solution at RT in 3 days (sample I). Its well-defined peaks (Figure 1a) could be precisely and purely indexed on a monoclinic structure, the most stable phase of tungsten oxides at RT,³⁴ in accordance with PDF no. 50-0233 of the ICDD library of spectra. Pecquenard et al.,²⁹ who are the pioneers in structural investigations of hydrated tungsten peroxide, reported that $[(\text{WO}_2)_2\text{O}_2\cdot\text{H}_2\text{O}]$ can be obtained only after heating at 120 °C,

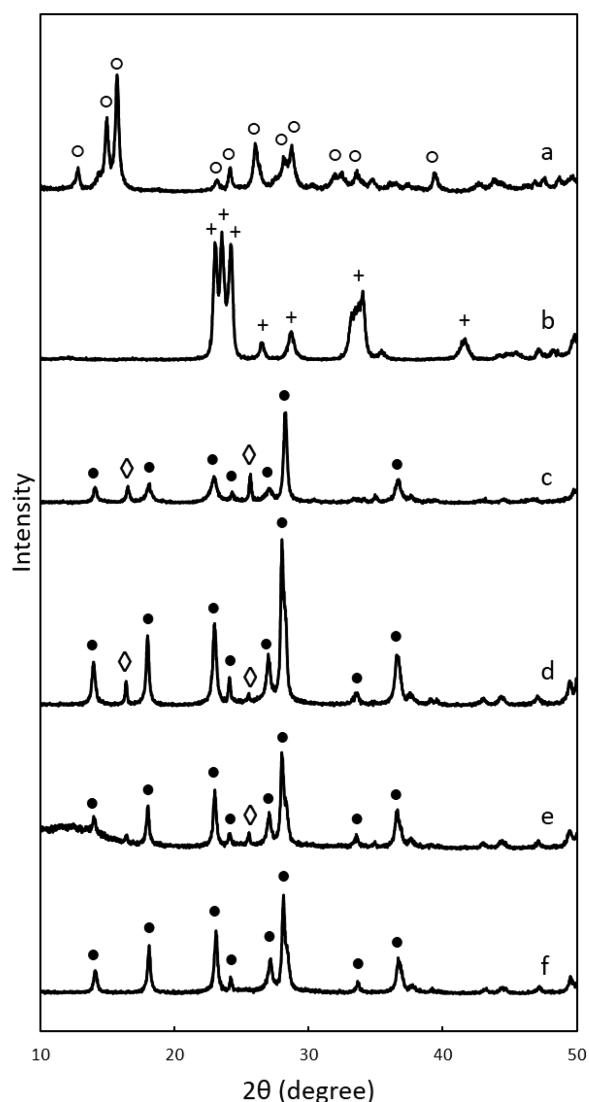


Figure 1. XRD patterns of (a) sample I, (b) sample II, (c) sample III, (d) sample IV, (e) sample V, and (f) sample VI. (○) $(\text{WO}_2)_2\text{O}_2\cdot\text{H}_2\text{O}$ (PDF no. 50-0233), (+) WO_3 (PDF no. 83-0950), (●) $\text{WO}_3\cdot 0.33\text{H}_2\text{O}$ (PDF no. 35-0270), and (◇) $\text{WO}_3\cdot\text{H}_2\text{O}$ (PDF no. 43-0679).

while at RT a more hydrated phase $[(\text{WO}_2)_2\text{O}_2\cdot\text{H}_2\text{O}]\cdot n\text{H}_2\text{O}$ is formed. Our synthesis method, however, made the formation of $[(\text{WO}_2)_2\text{O}_2\cdot\text{H}_2\text{O}]$ at RT in 3 days possible. Anhydrous WO_3 , another catalytically interesting structure, was obtained by decomposition and annealing of tungsten peroxide (sample I)^{35,36} via calcination at 600 °C (sample II, Figure 1b). The presence of {200}, {002}, and {020} reflections confirms that the obtained yellow powder was mainly composed of monoclinic WO_3 (PDF no. 83-0950).

Given the importance of associated water molecules of WO_3 ,³⁷ hydrated tungsten oxides were also synthesized (samples III–VI) via execution of higher thermal treatment (at 120 °C) in solution A, instead of the slow evaporation at RT, which resulted in a much shorter crystallization time, as well as changing the crystalline structure from monoclinic to orthorhombic (in comparison with samples I and II). Heating leads to quick decomposition of the water-soluble amorphous particles of solution A and production of insoluble solids with crystalline structures. The XRD pattern of sample III (Figure 1c) shows that it is composed of $\text{WO}_3\cdot 0.33\text{H}_2\text{O}$ (PDF no. 35-

0270) and $\text{WO}_3\cdot\text{H}_2\text{O}$ (tungstite; PDF no. 43-0679). The high intensity of the peaks at $2\theta = 28.3, 23.1, 36.8,$ and 18.1° demonstrates domination of the less hydrated phase; however, the main reflections of tungstite at $2\theta = 25.7$ ($\{111\}$) and $2\theta = 16.5$ ($\{020\}$) are also observed with less intensity. Both phases possess an orthorhombic crystalline structure.

Adding CTAB to the synthesis mixture reinforced the dominance of $\text{WO}_3\cdot 0.33\text{H}_2\text{O}$, evidence for which is the gradual diminishing of the intensities of the two mentioned peaks of tungstite, in samples IV, V, and VI (Figure 1d, e, and f), insofar as 100% pure $\text{WO}_3\cdot 0.33\text{H}_2\text{O}$ (PDF no. 35-0270) was obtained in sample VI (CTAB/W = 0.25; Figure 1f). This phase of tungsten oxide has been emphasized as being very sensitive to the synthesis conditions.^{25,38} The reported synthesis methods in the literature are considerably more complicated and time-consuming than the presented method. In fact, a role of structure directing agent (SDA) can be considered for CTA^+ cations in this synthesis method that directed the crystals to form a pure orthorhombic $\text{WO}_3\cdot 0.33\text{H}_2\text{O}$ structure in sample VI.

3.1.2. Spectral Analysis. Since the XRD technique revealed the bulk chemical structure of the obtained samples, FTIR analysis was employed to learn more about the composition of the organic part of the samples as well as different available tungsten bonds in crystalline structures of the samples. FTIR spectra of the samples are shown in Figure 2 and assignments of the considerable absorption bands are listed in Table S1 (Supporting Information).

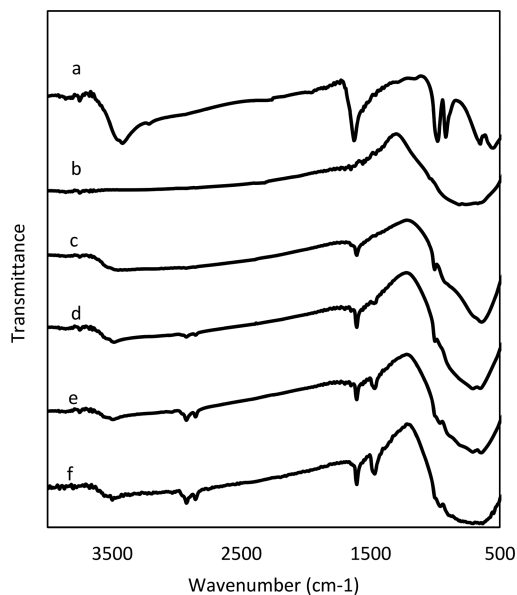


Figure 2. FTIR spectra of (a) sample I, (b) sample II, (c) sample III, (d) sample IV, (e) sample V, and (f) sample VI.

All the samples exhibit a strong peak located at $641\text{--}672\text{ cm}^{-1}$ which is assigned to the stretching vibration of a bridging oxygen atom between two tungsten atoms $\nu(\text{W}\text{--}\text{O}\text{--}\text{W})$.^{37,39–41} Generally, spectra of all the synthesized crystalline powders are very similar in the low-frequency region, except for sample I, which shows two more peaks at 548 and 919 cm^{-1} . These peaks, which are respectively assigned to tungsten-peroxo ($\text{W}(\text{O})_2$) and peroxo ($\text{O}\text{--}\text{O}$) groups, are typical vibration bands of peroxotungstic acid.⁴⁰ The peak located at $950\text{--}1004\text{ cm}^{-1}$, which is sharp in sample I and poorly resolved

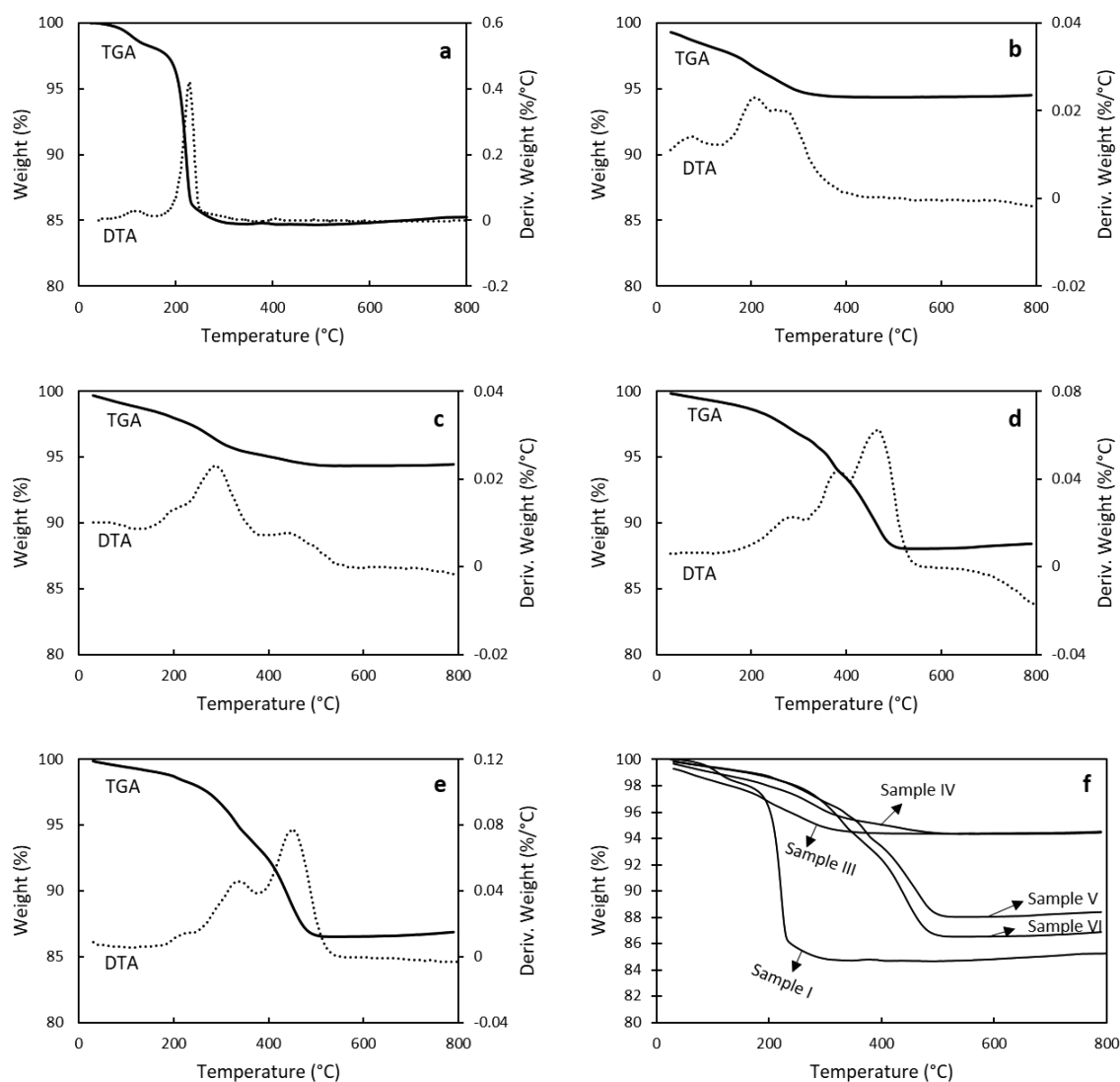


Figure 3. (a–e) TGA and DTA curves of (a) sample I, (b) sample III, (c) sample IV, (d) sample V, and (e) sample VI. (f) All the TGA curves.

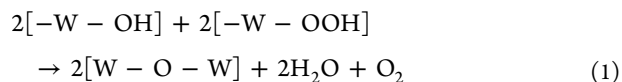
in other hydrated tungsten oxides (samples III–VI), is ascribed to the stretching mode of the terminal $W=O$ double bond.^{37,40,42,43}

Obviously, the peak(s) between 600 and 900 cm^{-1} is wider in the presence of CTA^+ cations (from sample IV to VI). The reason is the emergence of some peaks corresponding to $RN(CH_3)_3^+$ at 910 – 970 cm^{-1} ⁴⁴ and merging with the previous peaks. The spectra of CTAB-assisted synthesized samples (samples IV–VI) exhibit some additional peaks in the higher frequency region, where the vibration of organic compounds, as well as water molecules, is expected to appear. According to the literature, the peak at 1467 cm^{-1} can be attributed to $RN(CH_3)_3^+$, and the peaks at 2850 and 2927 cm^{-1} can be assigned to stretching vibrations of methyl ($-CH_3$) and/or methylene ($-(CH_2)-$) groups.⁴⁴ Although these peaks are weak in sample IV, their intensities increase with increasing CTAB content in the synthetic mixture for samples V and VI. The hydrated crystalline structures (samples I and III–VI) demonstrate a peak at 1606 – 1622 cm^{-1} and a peak at 3421 – 3491 cm^{-1} , which come from, respectively, bending and stretching vibrations of H_2O molecules.^{37,39,40}

3.1.3. Thermal Analysis. Thermogravimetric analysis (TGA) and differential thermal analysis (DTA) curves of the

synthesized samples are illustrated in Figure 3. Expectedly, anhydrous WO_3 (sample II) showed no essential weight loss during the thermal analysis up to 800 °C , and therefore, its curve is not included in Figure 3.

Initially, thermal analysis of sample III composed of only water and WO_3 (Figure 3b) indicates that the water molecules were expelled from the tungsten oxide structure at temperatures less than about 300 °C . After this temperature, the sample's weight, belonging to the WO_3 portion, remained constant. Gradually, expulsion of water that happened in a relatively wide temperature range ($25 < T < 300\text{ °C}$) comes from two main groups of the departed water molecules: (i) adsorbed and weakly bonded molecules that normally release at $T < 200\text{ °C}$ and (ii) HO and HO–O groups and strongly bonded molecules which, due to the inherent tendency of tungsten oxide to keep the water of hydration even at high temperatures, release at $200 < T < 300\text{ °C}$ as the reaction products of $W-OH$ and $W-OOH$ condensation:^{27,28}



The presence of abundant peroxide groups in sample I changed the behavior of the departure of water molecules (Figure 3a); its first weight loss at about 110 °C, similarly, comes from the departure of weakly bonded water molecules. However, more strongly bonded molecules departed the structure along with the peroxide group at about 220 °C, which resulted in more abrupt departure and greater weight loss compared to the other samples.

In the high temperature region ($T > 300$ °C), an additional weight loss is obtained only for the CTA⁺ containing samples (Figure 3c–e). This weight loss, which increases with CTA⁺ content in the synthesis mixture, corresponds to oxidation and consequent removal of CTA⁺ molecules that capped the surfaces of tungsten oxides. Quantitatively, 1.7, 8.7, and 10.0% weight losses (in $300 < T < 500$ °C) were obtained for samples IV, V, and VI, in which CTAB/W molar ratios of 0.1, 0.25, and 0.5 had been used in the synthetic solution, respectively. Differential thermal analysis indicated that removal of CTA⁺ took place in two main subtemperature ranges: (i) $300 < T < 350$ °C and (ii) $440 < T < 470$ °C.

Figure 3f compares TGA curves of all the samples together. As can be seen, at all temperatures less than 300 °C the curves of CTA⁺-capped samples (samples IV–VI) stay on top of that of sample III. This confirms lower water contents in the structures of samples IV–VI, concurring with the result of XRD.

3.1.4. Other Aspects of the Synthesized Samples. The high concentration of charged species and functional groups (and their probable ionization) in the synthesis medium,³⁰ as well as not using an autoclave in the employed pseudohydrothermal synthesis method, could mainly affect the morphologies and surface areas of the resultant solids.

Figures 4 and 5 display representative TEM images of the samples. NPs of (WO₂)O₂·H₂O (sample I, Figure 4a and b) tend to form into irregular-shaped substructures due to the high concentration of peroxo groups on their surface. First, the presence of many hydrogen ions in the precursor solution has

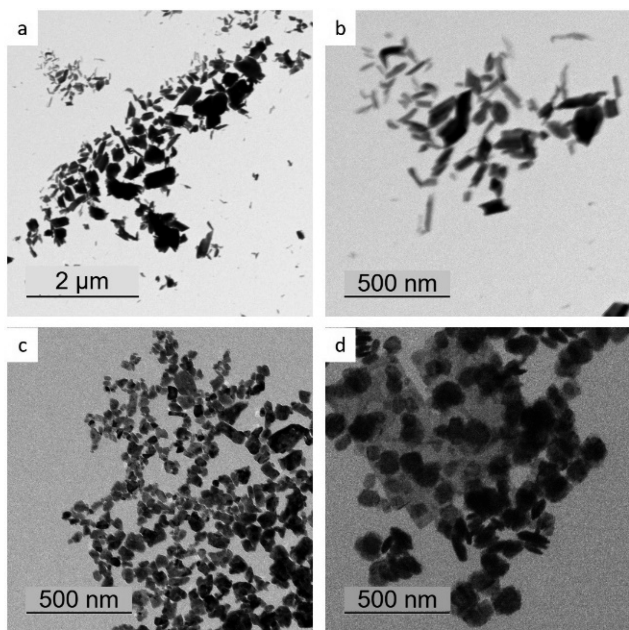


Figure 4. TEM images of (a and b) sample I (with different magnifications), (c) sample II, and (d) sample III.

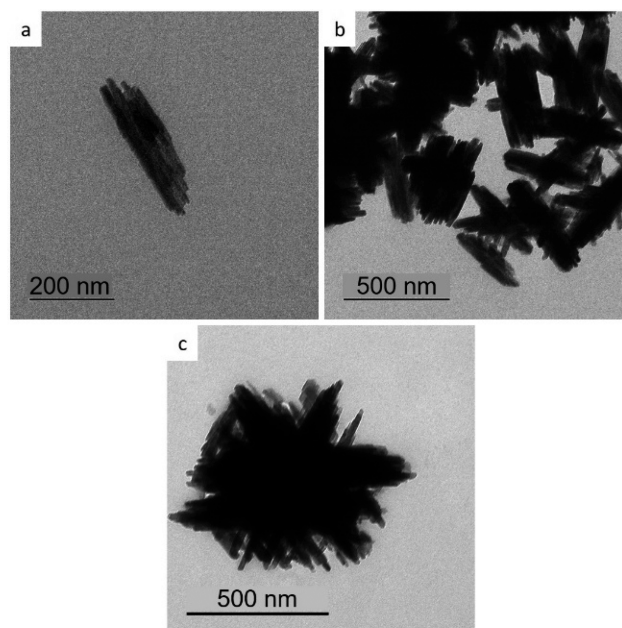


Figure 5. TEM images of (a) sample IV, (b) sample V, and (c) sample VI.

been reported, which increases the aggregation of tungsten oxide NPs.⁴⁵ Moreover, control of morphology to form a stable coordinated structure in the presence of H₂O₂ could be difficult due to the chelating feature of peroxo ligands [O₂]²⁻.²⁵ It makes more sense given the fact that no autoclave was used for hydrothermal treatment. Indeed, this chelating property of [O₂]²⁻ ligands has been well thought out as the fountainhead of H₂O₂'s role in the synthesis,²⁵ which led to complete dissolution of WO₃ in hydrogen peroxide and formation of a transparent tungsten peroxide solution, while WO₃ is not soluble in water.

With calcining at 600 °C and removal of hydrogen peroxide, monoclinic WO₃ NPs with platelet-like morphology with an average size of ~40 nm were obtained (sample II, Figure 4 c). Thermal treatment at higher temperatures had little influence on the overall morphology of the product. As shown in Figure 4d, the typical structure of sample III is a mixed morphology of nanoplatelet and nanorod, most likely due to the coexistence of two crystalline phases WO₃·0.33H₂O and WO₃·H₂O, and the platelet structure is somehow similar to sample II.

With the addition of CTAB to the synthesis medium, nanoneedle aggregates were formed (Figure 5), a typical morphology for WO₃·0.33H₂O that has been obtained before via more complicated and longer procedures.^{25,38} Changing the amount of CTAB, however, did not have a significant effect on the morphology of the products. Only, it seems that at higher concentrations of CTAB the particles showed slightly more tendency to aggregate. As a consequence, the specific surface area decreased from 17 m²/g in sample III to about 4 m²/g in sample VI. Table S2 in the Supporting Information lists the BET surface areas of the samples. The higher surface area of sample II (~29 m²/g) compared to the other samples highly likely arises from its calcination at a higher temperature, which removed all the surface functional groups, and therefore its NPs strongly avoid aggregation, as can be seen in its TEM image (Figure 4c).

Our efforts to organo-functionalize the tungsten oxides with anionic surfactants (e.g., acetic and valeric acids, instead of

CTAB) failed (as TGA and FTIR analyses confirmed), because the anionic functional groups at the head of these surfactants were repelled by the negatively charged surface of tungsten oxide. Evidence for this negative charge was obtained by measuring the zeta potential of the NPs dispersed in solution A (without CTAB, pH 1.6–1.8, Figure 6). The available

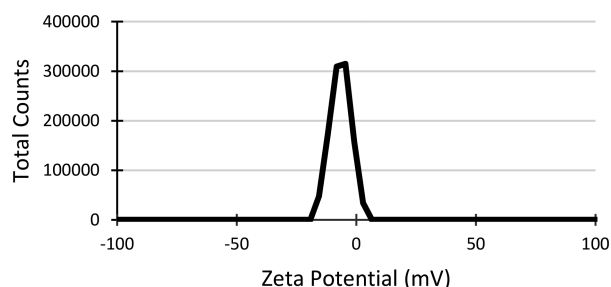


Figure 6. Surface zeta potential distribution of tungsten oxide NPs dispersed in the synthesis solution without adding CTAB at pH 1.6–1.8.

negatively charged species on the surface mainly consists of peroxy (O_2^{2-}) and hydroxyl (OH^-) groups (see Figure 2 and well-resolved absorption band of peroxy at 919 cm^{-1}). The presence of such a band in Figure 2c, although very weak, confirms that even after heating at $120\text{ }^\circ\text{C}$, there are still some O_2^{2-} ligands on the surface, while the $\text{W}(\text{O}_2)$ absorption band (548 cm^{-1}) has vanished.

3.2. Catalytic Test Results. Table 2 shows the conversion of oleic acid and yields of production of azelaic and pelargonic acids (Y_{AA} and Y_{PA} , respectively) over different synthesized catalysts with H_2O_2 as an oxidant after 5 h of reaction at $120\text{ }^\circ\text{C}$. The catalytic test results presented are the average of at least three runs over each catalyst. See the Supporting Information for more details about the quantitative analysis (section S2.2).

3.2.1. Influence of Different Catalysts on the Reaction. The first catalytic test was done without any catalyst (Table 2, entry 1); a modest 41% conversion and tiny yield percentages ($\leq 4\%$) confirmed that the benign used oxidant is not adequately efficient alone. To compare our catalysts' activities with a standard condition, a commercial tungsten oxide (WO_3 , 99.8%, Alfa Aesar Co.) was employed as a catalyst, also (entry 2), which, although significantly increasing the conversion ($\sim 90\%$), still resulted in low yields (less than 20%). Compared

to the commercial WO_3 , our prepared tungsten oxides showed much better efficiencies (entries 3–8). Complete conversion of initial oleic acid was obtained for all the samples after 5 h of reaction time, with high yields particularly for samples I, V, and VI.

The high catalytic efficiency of sample I (entry 3, 71 and 67% Y_{AA} and Y_{PA} , respectively) comes from the tungsten-peroxy (as seen by its XRD and FTIR) with a high concentration (as its TGA showed) in its structure $[(\text{WO}_2)\text{O}_2\cdot\text{H}_2\text{O}]$. Such peroxy complexes have been mentioned in the literature as shouldering the responsibility of advancing UFAs' oxidative cleavage reactions.^{3,14,16,18} Except for sample I, other samples were composed of tungsten trioxide, in anhydrous (sample II) or hydrated (samples III–VI) forms. Sample II in spite of advantages of higher WO_3 content (Table 2) and surface area (Table S2), as well as more uniform morphology and smaller particle size (Figure 4), yielded lower values compared to sample III (entries 4 and 5). The reason could be well ascribed to the important role of the linked water molecules of sample III ($\text{WO}_3\cdot 0.33\text{H}_2\text{O}$ and $\text{WO}_3\cdot\text{H}_2\text{O}$), which can increase in situ production of instant tungsten-peroxy groups during the reaction. It has been shown that the oxidation extent of tungsten trioxide in the presence of H_2O_2 (to produce tungsten-peroxy) decreases with a decrease in the content of water in its structures.³⁷

Samples IV–VI, however, did not generally comply with this trend (entries 6–8). As discussed in section 3.1.1, adding CTAB favored the formation of the less hydrated phase ($\text{WO}_3\cdot 0.33\text{H}_2\text{O}$), and accordingly, it was expected that the oxidative capabilities of the samples and, consequently, their catalytic efficiencies decrease by adding CTAB. But, except for sample IV, the two other CTA^+ -capped samples (V and VI) exhibited higher yields compared to sample III. The reason directly comes from the presence of CTA^+ , which tunes the surface state of the tungsten oxide and greatly affects its catalytic activity. Samples IV–VI, despite very slight structural differences in crystallinity (Figure 1), morphology (Figure 5), and WO_3 content (Table 2), exhibited significantly different yields. The CTA^+ molecules that capped the hydrophilic surface of $\text{WO}_3\cdot 0.33\text{H}_2\text{O}$ could make it partly hydrophobic and, hence, give it increased surface affinity to adsorb the organic substrate, oleic acid, molecules in the reaction medium. Admittedly, a higher concentration of oleic acid on the surface of the catalyst, where tungsten-peroxy species are accumulated, results in more reactant collision and consequently increases the reaction

Table 2. Catalytic Tests Results (Conversion of Oleic Acid and Yields of Production of Desired Products) and Weight Fractions of WO_3 in the Catalysts As the Assumed Active Sites

entry	catalyst (tungsten oxide)	chemical structure	WO_3 weight fraction in the catalyst (%) ^a	conversion (%) ^b	Y_{AA} (%) ^c	Y_{PA} (%) ^c
1				41	2	4
2	commercial	WO_3		91	10	18
3	sample I	$(\text{WO}_2)\text{O}_2\cdot\text{H}_2\text{O}$	84.9	100	71	67
4	sample II	WO_3	100.0	100	41	39
5	sample III	$\text{WO}_3\cdot 0.33\text{H}_2\text{O}$ and $\text{WO}_3\cdot\text{H}_2\text{O}$	94.5	100	51	53
6	sample IV	$\text{WO}_3\cdot 0.33\text{H}_2\text{O} \gg \text{WO}_3\cdot\text{H}_2\text{O}$	94.3	100	39	37
7	sample V	$\text{WO}_3\cdot 0.33\text{H}_2\text{O} \gg \text{WO}_3\cdot\text{H}_2\text{O}$	88.1	100	77	69
8	sample VI	$\text{WO}_3\cdot 0.33\text{H}_2\text{O}$	86.5	100	60	64

^aWeight fraction of WO_3 , assumed as an active site (regardless of current vast challenges on the nature of catalytic centers in metal oxide catalysis), was calculated from quantitative analysis of TGA data. ^bReaction conditions: time, 5 h; temperature, $120\text{ }^\circ\text{C}$; solvent, tert-butanol; initial amounts of oleic acid, 1 g; t-butanol, 7.5 mL; H_2O_2 , 4 mL; catalyst, 0.45 g; agitation rate, $\sim 400\text{ rpm}$. ^cY: Yield (molar), in this work, is defined as the amount of a product formed per total amount of oleic acid consumed (both in moles; Y_{AA} , yield of azelaic acid; Y_{PA} , yield of pelargonic acid).

efficiency (happened for samples V and VI). However, the presence of long-chain CTA⁺ on the surface is a double-edged sword; apart from the positive effect of hydrophobization, it would lead to a steric repulsion effect, which considering molecular geometry of CTA⁺ and oleic acid, could prevent oleic acid from approaching the surface. The competition between these two positive and negative effects, which depends on the density of CTA⁺ on the surface, gives rise to the different yields obtained by samples IV, V, and VI; it seems that low density of CTA⁺ in sample IV could not provide enough hydrophobicity, and the steric repulsion forces resulted in lower yields (entry 6), while at the higher density (sample VI), the provided hydrophobicity overcame the increase in steric repulsion effects, resulting in higher yields (entry 8). The optimized density of CTA⁺ on the surface, giving 77% Y_{AA} (entry 7), was obtained when a CTAB/W molar ratio of 0.25 was used in the synthesis (sample V). The obtained reaction efficiencies in this work seem interesting when being compared with the previously reported heterogeneous catalytic oxidative cleavage of oleic acid.^{5,17,19}

Given the improved compatibility of the solid catalysts with reactants, resulting in deservedly ascribing a phase transfer role to the organo-functionalized tungsten oxides, further works are currently underway in our laboratory to reduce (or even eliminate) the reaction solvent.

3.2.2. Effects of Temperature and Time on the Reaction. Sample V was subjected to an investigation of the effects of reaction temperature and time. Employing a less reaction temperature (85 °C) resulted in a slightly lower conversion (92%) and moderately lower Y_{AA} and Y_{PA} (49 and 47%, respectively). Since complete conversion of oleic acid was obtained at 120 °C, temperatures higher than this, which would cause decomposition of hydrogen peroxide, were not tried. To study H₂O₂ loss during the reaction through catalytic or thermal decomposition, some catalytic tests without oleic acid were carried out, and then H₂O₂ loss was calculated by titrimetry. Results showed a 22% loss in the absence of any catalyst and 30–70% in the presence of the synthesized catalysts after 5 h of reaction at 120 °C.

Employing shorter reaction times resulted in a significantly lower conversion. After 3 h of reaction at 120 °C, over sample V, 58% of the initial oleic acid was converted to azelaic and pelargonic acids with yields of 62 and 59%, respectively. A longer reaction time (7.5 h) caused the yields to slightly reduce, most probably due to degradation of azelaic and pelargonic acids caused by prolonged heating in the presence of the catalyst.¹⁹ Further works to optimize the reaction temperature and time for all the samples via kinetic studies are ongoing in our lab and will be presented in another article.

3.2.3. Recyclability of the Catalysts. All the synthesized catalysts were recovered after the reactions and reused to examine their recyclability. Up to four cycles, they all showed more than 97% conversion without a significant loss in the yields, except for sample I, which showed a considerable decrease in catalytic efficiency after the first cycle. Figure 7 compares the yields of production of azelaic acid in four cycles. Almost the same trend was obtained for Y_{PA} .

FTIR analysis was performed on the catalysts after each cycle to probe any change in their chemical structures. Except sample I, other catalysts exhibited almost the same FTIR patterns as their original spectra (Supporting Information, Figures S9–S14) confirming that they essentially keep their chemical natures during the reaction. This chemical stability is because

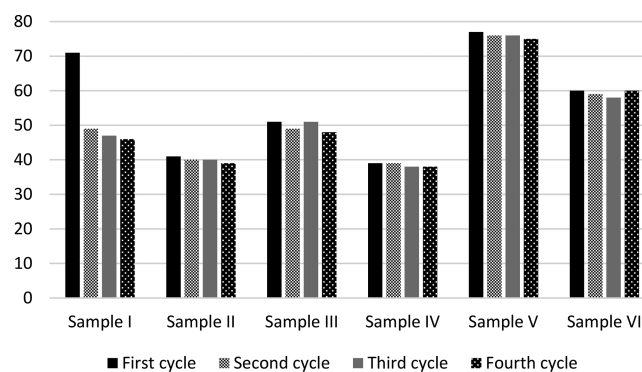


Figure 7. Recyclability of the synthesized catalysts; yields of production of azelaic acid over the synthesized catalysts in fourth cycles (reaction conditions: time, 5 h; temperature, 120 °C; solvent, *tert*-butanol; initial amounts of oleic acid, 1 g; *t*-butanol, 7.5 mL; H₂O₂, 4 mL; catalyst, 0.45 g; agitation rate, ~400 rpm).

the catalysts had been already exposed to a thermal treatment at high temperatures (600 °C for sample II and 120 °C for sample III to VI) during the synthesis procedure, whereas the structure of sample I, which had been synthesized at RT, was dramatically changed after the first cycle. Evidence for this was found in its FTIR analysis, before and after the reaction (Figure S9), as well as XRD analysis (Figure S15), where the disappearance of the corresponding peaks of [(WO₂)₂O₂·H₂O], and instead, emergence of the characteristic peaks of WO₃·0.33H₂O (PDF no. 87-1203) imply decomposition of intercrystalline tungsten-peroxo species during the reaction. This gives rise to a significant loss of catalytic efficiency of sample I after the first reaction cycle.

In order to examine leaching of WO₃ species and the true heterogeneity of the reaction, a catalytic test was performed over sample V, which had given the highest yields, and was stopped after 2.5 h of reaction. After cooling down and removal of the catalyst, the reaction mixture was exposed to the reaction conditions for the remaining reaction time (2.5 h). In the second 2.5 h, conversion slightly increased (from 43% to 51%), as a result of oxidant ability in advancing the reaction alone (see entry 1 of Table 2), while changes in the yields were negligible. Moreover, for all the samples, weight loss of the catalyst after each reaction cycle was exactly measured (Supporting Information, Table S3). Generally, the catalysts' weight losses were less than ~2%, with the minimum values, interestingly, obtained for the organo-functionalized catalysts (particularly samples V and VI), most likely because of the hydrophobization effects making the CTA⁺-capped catalysts more water-tolerant with less leaching of inherently hydrophilic active sites (WO₃). These results imply no significant leaching of active sites during the reaction.

4. CONCLUSIONS

A straightforward and green synthetic procedure, simply starting from cheap micrometer-scale W powder and adding H₂O₂, resulted in the formation of a clear solution of peroxotungstic species, which were then crystallized into different structures of tungsten oxide via altering temperature and/or adding CTAB. Given the potential of WO_x as an oxidizing catalyst, all the synthesized catalysts were adequately efficient to fully convert oleic acid after 5 h of reaction with H₂O₂ as a benign oxidant. Intriguingly, adding CTAB to the synthesis mixture not only played a structure-directing role

influencing the final product's crystalline phase but also stably capped the surfaces of tungsten oxide NPs, resulting in an improved compatibility of the solid catalyst with the organic substrate and aqueous oxidant, and consequently, enhancement of production yield of the desired azelaic acid up to just less than 80%. This result seems advantageous when being compared to the scarce works reported on heterogeneous catalytic oxidative cleavage of oleic acid. The organo-functionalization by an optimized amount of CTA⁺ could hydrophobically adjust the inherently hydrophilic surface of tungsten oxide, giving more surface affinity to adsorb oleic acid in the reaction. This, together with the solid nature and insolubility of WO₃, furnished the CTA⁺-capped catalyst with additional advantages of no significant leaching of active sites, convenient recovery, and steady reuse up to four cycles without a loss of activity. Hopefully, application of this catalytic process could be extended to other UFAs available in vegetable oils, which would make diacid production more economical, commercially attractive, and environmentally friendly.

■ ASSOCIATED CONTENT

■ Supporting Information

The Supporting Information is available free of charge on the ACS Publications website at DOI: 10.1021/acs.iecr.7b03001.

(S1) Characterization techniques, (S2) analysis of the reaction products, (S2.1) sample preparation for GC-MS analysis, (S2.2) quantitative analysis, (S2.3) GC-MS specifications, (Figures S1–S8) gas chromatograms of products, (Figures S9–S14) FTIR spectra of the samples after different reaction cycles, (Figure S15) XTD pattern of sample I after reaction, (Table S1) assignments of the FTIR absorption bands of the prepared samples, (Table S2) BET surface areas of the samples, (Table S3) weight losses of the catalysts after reaction cycles (PDF)

■ AUTHOR INFORMATION

Corresponding Author

*Tel.: +1 (418) 656-3774. E-mail: trong-on.do@gch.ulaval.ca.

ORCID

Amir Enferadi-Kerenkan: 0000-0002-8683-967X

Trong-On Do: 0000-0002-7785-5299

Author Contributions

All authors have given approval to the final version of the manuscript.

Notes

The authors declare no competing financial interest.

■ ACKNOWLEDGMENTS

This work was supported by the Natural Science and Engineering Research Council of Canada (NSERC) through the INNOV-UC and Discovery grants. The authors wish to thank the industrial partners (Oleotek and SiliCycle Inc.) for stimulating discussions and comments.

■ ABBREVIATIONS

NP, nanoparticle; UFA, unsaturated fatty acid; AA, azelaic acid; PA, pelargonic acid; XRD, X-ray diffraction; FTIR, Fourier transform infrared; TGA, thermogravimetric analysis; DTA, differential thermal analysis; TEM, transition electron microscopy

■ REFERENCES

- (1) Anneken, D. J.; Both, S.; Christoph, R.; Fieg, G.; Steinberner, U.; Westfechtel, A. Fatty Acids. In *Ullmann's Encyclopedia of Industrial Chemistry*; Wiley-VCH Verlag GmbH & Co. KGaA: Weinheim, 2000.
- (2) Köckritz, A.; Blumenstein, M.; Martin, A. Catalytic cleavage of methyl oleate or oleic acid. *Eur. J. Lipid Sci. Technol.* **2010**, *112*, 58.
- (3) Turnwald, S. E.; Lorier, M. A.; Wright, L. J.; Mucalo, M. R. Oleic Acid Oxidation Using Hydrogen Peroxide in Conjunction with Transition Metal Catalysis. *J. Mater. Sci. Lett.* **1998**, *17*, 1305.
- (4) Kulik, A.; Janz, A.; Pohl, M.-M.; Martin, A.; Köckritz, A. Gold-catalyzed synthesis of dicarboxylic and monocarboxylic acids. *Eur. J. Lipid Sci. Technol.* **2012**, *114* (11), 1327–1332.
- (5) Dapurkar, S. E.; Kawanami, H.; Yokoyama, T.; Ikushima, Y. Catalytic Oxidation of Oleic Acid in Supercritical Carbon Dioxide Media with Molecular Oxygen. *Top. Catal.* **2009**, *S2*, 707.
- (6) Santacesaria, E.; Sorrentino, A.; Rainone, F.; Di Serio, M.; Speranza, F. Oxidative Cleavage of the Double Bond of Monoenic Fatty Chains in Two Steps: A New Promising Route to Azelaic Acid and Other Industrial Products. *Ind. Eng. Chem. Res.* **2000**, *39*, 2766.
- (7) Spannring, P.; Prat, I.; Costas, M.; Lutz, M.; Bruijninx, P. C. A.; Weckhuysen, B. M.; Klein Gebbink, R. J. M. Fe(6-Me-PyTACN)-catalyzed, one-pot oxidative cleavage of methyl oleate and oleic acid into carboxylic acids with H₂O₂ and NaIO₄. *Catal. Sci. Technol.* **2014**, *4*, 708.
- (8) Spannring, P.; Yazerski, V.; Bruijninx, P. C. A.; Weckhuysen, B. M.; Klein Gebbink, R. J. M. Fe-Catalyzed One-Pot Oxidative Cleavage of Unsaturated Fatty Acids into Aldehydes with Hydrogen Peroxide and Sodium Periodate. *Chem. - Eur. J.* **2013**, *19*, 15012.
- (9) Behr, A.; Tenhumberg, N.; Wintzer, A. An efficient reaction protocol for the ruthenium-catalysed epoxidation of methyl oleate. *Eur. J. Lipid Sci. Technol.* **2012**, *114*, 905.
- (10) Behr, A.; Tenhumberg, N.; Wintzer, A. Efficient ruthenium-catalysed oxidative cleavage of methyl oleate with hydrogen peroxide as oxidant. *RSC Adv.* **2013**, *3*, 172.
- (11) Ho, C.-M.; Yu, W.-Y.; Che, C.-M. Ruthenium Nanoparticles Supported on Hydroxyapatite as an Efficient and Recyclable Catalyst for cis-Dihydroxylation and Oxidative Cleavage of Alkenes. *Angew. Chem., Int. Ed.* **2004**, *43*, 3303.
- (12) Rup, S.; Sindt, M.; Oget, N. Catalytic oxidative cleavage of olefins by RuO₄ organic solvent-free under ultrasonic irradiation. *Tetrahedron Lett.* **2010**, *51*, 3123.
- (13) Rup, S.; Zimmermann, F.; Meux, E.; Schneider, M.; Sindt, M.; Oget, N. The ultrasound-assisted oxidative scission of monoenic fatty acids by ruthenium tetroxide catalysis: Influence of the mixture of solvents. *Ultrason. Sonochem.* **2009**, *16*, 266.
- (14) Antonelli, E.; D'Aloisio, R.; Gambaro, M.; Fiorani, T.; Venturello, C. Efficient Oxidative Cleavage of Olefins to Carboxylic Acids with Hydrogen Peroxide Catalyzed by Methyltriethylammonium Tetrakis(oxodiperoxotungsto)phosphate(3-) under Two-Phase Conditions. Synthetic Aspects and Investigation of the Reaction Course. *J. Org. Chem.* **1998**, *63*, 7190.
- (15) Godard, A.; De Caro, P.; Thiebaud-Roux, S.; Vedrenne, E.; Mouloungui, Z. New Environmentally Friendly Oxidative Scission of Oleic Acid into Azelaic Acid and Pelargonic Acid. *J. Am. Oil Chem. Soc.* **2013**, *90*, 133.
- (16) Haimov, A.; Cohen, H.; Neumann, R. Alkylated Polyethyleneimine/Polyoxometalate Synzymes as Catalysts for the Oxidation of Hydrophobic Substrates in Water with Hydrogen Peroxide. *J. Am. Chem. Soc.* **2004**, *126*, 11762.
- (17) Kerenkan, A. E.; Ello, A. S.; Echchahed, B.; Do, T.-O. Synthesis of Mesoporous Tungsten Oxide/ γ -Alumina and Surfactant-Capped Tungsten Oxide Nanoparticles and Their Catalytic Activities in Oxidative Cleavage of Oleic Acid. *Int. J. Chem. React. Eng.* **2016**, *14*, 899.
- (18) Khlebnikova, T. B.; Pai, Z. P.; Fedoseeva, L. A.; Mattsat, Y. V. Catalytic oxidation of fatty acids. II. Epoxidation and oxidative cleavage of unsaturated fatty acid esters containing additional functional groups. *React. Kinet. Catal. Lett.* **2009**, *98*, 9.

- (19) Nouredдини, H.; Kanabur, M. Liquid-phase catalytic oxidation of unsaturated fatty acids. *J. Am. Oil Chem. Soc.* **1999**, *76*, 305.
- (20) Oakley, M. A.; Woodward, S.; Coupland, K.; Parker, D.; Temple-Heald, C. Practical dihydroxylation and C–C cleavage of unsaturated fatty acids. *J. Mol. Catal. A: Chem.* **1999**, *150*, 105.
- (21) Pai, Z. P.; Tolstikov, A. G.; Berdnikova, P. V.; Kustova, G. N.; Khlebnikova, T. B.; Selivanova, N. V.; Shangina, A. B.; Kostrovskii, V. G. Catalytic oxidation of olefins and alcohols with hydrogen peroxide in a two-phase system giving mono- and dicarboxylic acids. *Russ. Chem. Bull.* **2005**, *54*, 1847.
- (22) Enferadi Kerenkan, A.; Beland, F.; Do, T.-O. Chemically catalyzed oxidative cleavage of unsaturated fatty acids and their derivatives into valuable products for industrial applications: a review and perspective. *Catal. Sci. Technol.* **2016**, *6*, 971.
- (23) O'Neill, H. S. C.; Berry, A. J.; Eiggins, S. M. The solubility and oxidation state of tungsten in silicate melts: Implications for the comparative chemistry of W and Mo in planetary differentiation processes. *Chem. Geol.* **2008**, *255*, 346.
- (24) Jin, P.; Wei, D. H.; Wen, Y. Q.; Luo, M. F.; Wang, X. Y.; Tang, M. S. A combined experimental and DFT study of active structures and self-cycle mechanisms of mononuclear tungsten peroxo complexes in oxidation reactions. *J. Mol. Struct.* **2011**, *992*, 19.
- (25) Zhou, L.; Zou, J.; Yu, M.; Lu, P.; Wei, J.; Qian, Y.; Wang, Y.; Yu, C. Green Synthesis of Hexagonal-Shaped $\text{WO}_3 \cdot 0.33\text{H}_2\text{O}$ Nanodiscs Composed of Nanosheets. *Cryst. Growth Des.* **2008**, *8*, 3993.
- (26) Kudo, T.; Okamoto, H.; Matsumoto, K.; Sasaki, Y. Peroxopolytungstic acids synthesized by direct reaction of tungsten or tungsten carbide with hydrogen peroxide. *Inorg. Chim. Acta* **1986**, *111*, L27.
- (27) Deepa, M.; Kar, M.; Agnihotry, S. A. Electrodeposited tungsten oxide films: annealing effects on structure and electrochromic performance. *Thin Solid Films* **2004**, *468*, 32.
- (28) Deepa, M.; Srivastava, A. K.; Agnihotry, S. A. Influence of annealing on electrochromic performance of template assisted, electrochemically grown, nanostructured assembly of tungsten oxide. *Acta Mater.* **2006**, *54*, 4583.
- (29) Pecquenard, B.; Castro-Garcia, S.; Livage, J.; Zavalij, P. Y.; Whittingham, M. S.; Thouvenot, R. Structure of Hydrated Tungsten Peroxides $[\text{WO}_2(\text{O}_2)\text{H}_2\text{O}] \cdot n\text{H}_2\text{O}$. *Chem. Mater.* **1998**, *10*, 1882.
- (30) Redel, E.; Petrov, S.; Dag, Ö.; Moir, J.; Huai, C.; Mirtchev, P.; Ozin, G. A. Green Nanochemistry: Metal Oxide Nanoparticles and Porous Thin Films from Bare Metal Powders. *Small* **2012**, *8*, 68.
- (31) Metcalfe, L. D.; Schmitz, A. A. The Rapid Preparation of Fatty Acid Esters for Gas Chromatographic Analysis. *Anal. Chem.* **1961**, *33*, 363.
- (32) Metcalfe, L. D.; Schmitz, A. A.; Pelka, J. R. Rapid Preparation of Fatty Acid Esters from Lipids for Gas Chromatographic Analysis. *Anal. Chem.* **1966**, *38*, 514.
- (33) Okamoto, H.; Yamanaka, K.; Kudo, T. Protonic conduction and electrochromism of amorphous peroxopolytungstic acid. *Mater. Res. Bull.* **1986**, *21*, 551.
- (34) Salje, E.; Viswanathan, K. Physical properties and phase transitions in WO_3 . *Acta Crystallogr., Sect. A: Cryst. Phys., Diffr., Theor. Gen. Crystallogr.* **1975**, *31*, 356.
- (35) Kudo, T. A new heteropolyacid with carbon as a heteroatom in a Keggin-like structure. *Nature* **1984**, *312*, 537.
- (36) Meulenkamp, E. A. Mechanism of WO_3 Electrodeposition from Peroxy-Tungstate Solution. *J. Electrochem. Soc.* **1997**, *144*, 1664.
- (37) Lu, Y.; Yin, H.; Wu, H.; Liu, H.; Jiang, T.; Wada, Y. Structural effect of tungsten oxides on selective oxidation of cyclopentene to glutaraldehyde. *Catal. Commun.* **2006**, *7*, 832.
- (38) Gerand, B.; Nowogrocki, G.; Figlarz, M. A new tungsten trioxide hydrate, $\text{WO}_3 \cdot 13\text{H}_2\text{O}$: Preparation, characterization, and crystallographic study. *J. Solid State Chem.* **1981**, *38*, 312.
- (39) Huo, L.; Zhao, H.; Mauvy, F.; Fourcade, S.; Labrugere, C.; Pouchard, M.; Grenier, J.-C. Synthesis and mixed conductivity of ammonium tungsten bronze with tunneling structures. *Solid State Sci.* **2004**, *6*, 679.
- (40) Pecquenard, B.; Lecacheux, H.; Livage, J.; Julien, C. Orthorhombic WO_3 Formed via a Ti-Stabilized $\text{WO}_3 \cdot 13\text{H}_2\text{O}$ Phase. *J. Solid State Chem.* **1998**, *135*, 159.
- (41) Zavalij, P.; Guo, J.; Whittingham, M. S.; Jacobson, R. A.; Pecharsky, V.; Bucher, C. K.; Hwu, S.-J. Keggin Cluster Formation by Hydrothermal Reaction of Tungsten Trioxide with Methyl Substituted Ammonium: The Crystal Structure of Two Novel Compounds, $[\text{NH}_2(\text{CH}_3)_2]_6\text{H}_2\text{W}_{12}\text{O}_{40} \cdot \sim 4\text{H}_2\text{O}$ and $[\text{N}(\text{CH}_3)_4]_6\text{H}_2\text{W}_{12}\text{O}_{40} \cdot 2\text{H}_2\text{O}$. *J. Solid State Chem.* **1996**, *123*, 83.
- (42) Hashimoto, M.; Koyano, G.; Mizuno, N. In Situ IR Spectrum of 12-Tungstophosphoric Acid Hexahydrate with Planar H_5O_2^+ . *J. Phys. Chem. B* **2004**, *108*, 12368.
- (43) Zayat, M.; Reinfeld, R.; Minti, H.; Orel, B.; Svegl, F. Gasochromic Effect in Platinum-Doped Tungsten Trioxide Films Prepared by the Sol-Gel Method. *J. Sol-Gel Sci. Technol.* **1998**, *11*, 161.
- (44) Huang, L.; Chen, X.; Li, Q. Synthesis of microporous molecular sieves by surfactant decomposition. *J. Mater. Chem.* **2001**, *11*, 610.
- (45) Pang, H.-F.; Xiang, X.; Li, Z.-J.; Fu, Y.-Q.; Zu, X.-T. Hydrothermal synthesis and optical properties of hexagonal tungsten oxide nanocrystals assisted by ammonium tartrate. *Phys. Status Solidi A* **2012**, *209*, 537.